Acta Crystallographica Section D
**Biological Crystallography**
ISSN 0907-4449

# X-ray beam/biomaterial thermal interactions in third-generation synchrotron sources

**Tuncer M. Kuzay,† Michael Kazmierczak*‡ and B. J. Hsieh**

Advanced Photon Source, Argonne National Laboratory, 9700 South Cass Avenue, Argonne, Illinois 60439, USA

† Deceased.
‡ On sabbatical leave from University of Cincinnati, Department of Mechanical, Industrial and Nuclear Engineering, Cincinnati, Ohio 45221-0072, USA.

Correspondence e-mail: mike.kazmierczak@uc.edu

Received 27 April 2000
Accepted 10 September 2000

Third-generation synchrotron sources generate strong X-ray beams. The beam's interaction with biomaterials gives rise to concerns related to thermal damage and radiation damage. Of the two issues, the thermal interaction is conducive to rigorous analysis from first principles, although this has not been performed to date in a comprehensive manner. In this study, the interaction of the X-ray beam emanating from a third-generation synchrotron with a typical frozen biocrystal is theoretically studied, focusing specifically on the resulting unsteady (time-dependent) and steady heat-transfer phenomena. A unique regime map is developed to explain and to identify, on the basis of Fourier and Biot numbers as governing parameters, the applicable mathematical models that predict the subsequent thermal behavior. Depending on the values of these parameters, some simplified but realistic 'generic' solutions are generated that are suitable for that particular domain of applicability. Classical heat-transfer theory was used to describe the third-generation X-ray beam and biomaterial thermal interaction. Besides the generalized approach presented, numerous illustrative cases were solved and the resulting temperature levels are explicitly presented. Overall, the resulting thermal behavior of the system, *i.e.* peak and local temperature distribution, during both early transient development and for sustained long-time steady-state conditions, depends on a number of factors including the amount of energy absorbed, convective heat-transfer film coefficient and gas temperature, the sample size and shape, and the thermophysical properties of the sample and cooling gas. Results of the analysis revealed the strong influence that convection has on the transient and final steady-state temperature of the sample and the impact of internal heat conduction. The characteristic timescales of the important and dominant thermal processes with respect to the two types of thermal models are clearly identified.

## 1. Introduction

Damage to biological specimens from synchrotron X-ray beams has been a subject of research for the past 20 years or so. Both thermal and radiation damage scenarios have been considered. The thermal problem stems from the consideration of direct energy deposition in the specimen as a portion or all of the beam is absorbed in the material. The radiation damage is thought to stem from the ionizing aspect of the X-ray beams. By consensus, the radiation damage occurs in two phases (Blake & Phillips, 1962; Gonzalez & Nave, 1994; Nave, 1995). In the primary phase, energetic photons from the beam interact with the molecular structure of the specimen.

The energy of interaction causes increased thermal vibration of the molecules and can cause breakage of atomic bonds in the molecule thus creating 'free radicals'. The deposited energy drives these radicals from the primary site into the specimen causing further damage to the structure as a secondary effect. Such effects in the form of radiation damage have a much stronger impact on soft condensed matter, such as biological systems, in which thermodynamic effects, free-radical formation and migration can be easily induced. In addition, most biological specimens contain water. The radiolytic effects arising from the destruction of water molecules in the specimen by intense X-rays are profound.

While a systematic general theory on the radiation damage to biosamples does not exist, it has been experimentally well established that cryogenic cooling of the biosamples to about 100 K or so can at least mitigate the damage for most studies in second- and third-generation synchrotron X-ray beams (Hope *et al.*, 1989; Garman & Schneider, 1997; Garman, 1999). Biosamples in such experiments are usually soaked in a cryoprotectant prior to cryocooling so that the water is not converted to ice hence damaging the sample during the accompanying dilation. The water is thus maintained in a 'supercooled' vitrified state with no volumetric change (Teng, 1990; Lock, 1990). From this broad phenomenological discussion of the damage issue, the thermal and radiation damage are clearly linked, at least in the primary effect phase of the beam/material interaction. It should also be noted that the thermal effect can be much more easily theoretically modeled. The main purpose of this paper is to model such thermal transport for biosamples for the third-generation synchrotron beams.

The authors are unaware of a clear and complete thermal analysis of this problem, which is surprising since the problem is of such great interest to macromolecular crystallographers and moreover the solution methodology is straightforward. To date, the only thermal treatment we have seen in the literature that deals with the problem of this type is the adiabatic thermal model (Helliwell, 1992), which has been used mainly only to provide a rough estimate of the sample's maximum temperature rise (Anfinrud, 1999; Srajer *et al.*, 1996; Ren *et al.*, 1999). In the present study, we thermally analyze the given problem in a fairly rigorous but as simple a manner as possible employing the principles of classical heat-transfer theory and present the information to synchrotron users in an organized manner. To this end, we will first broadly classify and categorize the two different 'thermal model types' and identify their range of validity *via* the help of a novel heat-transfer 'thermal regime' map. We then analyze in detail two specific test problems (*i.e.* thin and thick samples) to help illustrate the thermophysics while providing some 'real and useful' numbers.

## 2. System of interest

The biosample treated here is typical of the biocrystals used in cryocooled crystallography studies: namely, the crycooled sample is held in a twisted fiber loop and is subjected to an oncoming X-ray beam while being cooled convectively *via* an annular nitrogen-gas stream from a cryostat, as shown in Fig. 1. Given this configuration, the biocrystal is *internally* heated as the energy from the X-ray beam is absorbed and is *externally* cooled from the front and rear surfaces by convection to the cold $N_2$ gas stream. The target area of the beam is assumed to be larger than the maximum lateral dimension of the crystal, thus allowing the one-dimensional plane layer simplification shown (assuming negligible cooling to the base pin through the fiber). Both thin and thick crystals are considered, as the formalism in the theoretical modeling is different for these two cases. The thin crystal can be treated as spatially uniform as a pure 'lumped model'. Hence, the resulting temperature in the sample is a simple time function. The thick crystals' temperature will, on the other hand, manifest both spatial and temporal variation, *i.e.* a 'distributed model'.

The temperature response (in time and space) of the sample can be calculated readily. Classical heat-transfer theory holds without question since the temporal and spatial dimensions of the X-ray beam (even that emanating from a third-generation synchrotron source) are much larger than the internal energy transport carriers, *i.e.* electrons and phonons, of the biomatter itself. Furthermore, note that in this analysis the exact detailed pulse-like structure of the X-ray beam arising from the different loading scheme of the synchrotron storage ring can also be ignored and effectively replaced with a constant appropriately 'time-averaged' power of the absorbed X-ray beam, *i.e.* a time-independent thermal input source is used in the thermal models. Note that this approximation is valid since the timescales of thermal diffusion and convection/thermal storage combination, ranging from milliseconds to seconds, is so much longer than the pulse width and pulse spacing of the X-ray beam, nanoseconds to microseconds, found in typical third-generation sources.

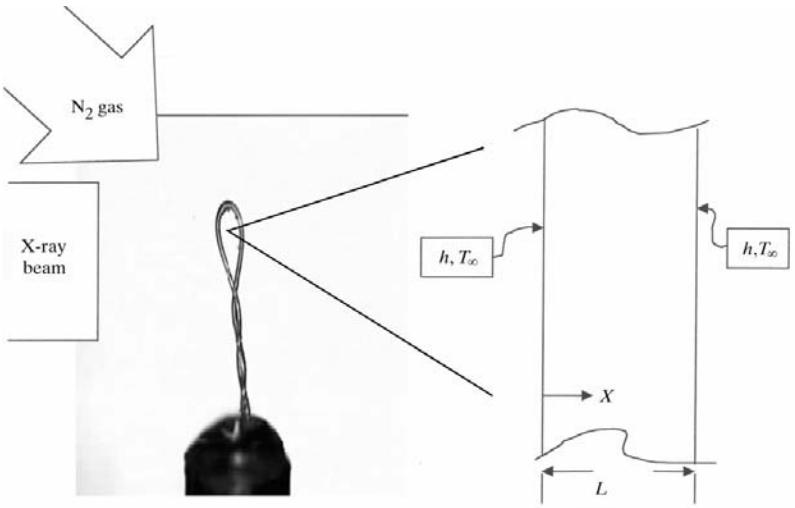


**Figure 1**
Biocrystal geometry modeled as a one-dimensional plane layer.

## 3. Regime map to identify applicable mathematical model

Before beginning the thermal calculation for the problem at hand, one must decide on the appropriate mathematical formulation to use. Problems in transient heat transfer can be classified as falling into two main categories: 'lumped' or 'distributed'. In the lumped system, the internal temperature gradients in the body are assumed to be negligible and hence the temperature within the whole body is approximated by a single temperature that changes with time $T(t)$. In contrast, the temperature in a distributed system is non-uniform in space and varies in time and position $T(x, t)$. Nomenclature is given in Table 1.

Clearly, the distributed model represents the more realistic heat-transfer behavior, but the lumped-model formulation is significantly easier to solve, leading to an ordinary differential equation *versus* a partial differential equation. It has been shown (Bejan, 1993) that in many cases the lumped-model simplification is often a very good approximation and is reasonably valid under certain conditions. These conditions are best expressed in terms of two dimensionless parameters, namely the Biot and Fourier numbers, such that

$$\begin{aligned} &\text{for Bi} < 0.02 \text{ and Fo} > 0.02 \\ &\text{the lumped model is valid,} \end{aligned} \tag{1}$$

where

$$\text{Bi} = hL/k = R_{\text{cond}}/R_{\text{conv}} = (L/kA)/(1/hA) \tag{2}$$

and

$$\text{Fo} = t/t_d = t/(L^2/\alpha) = t\alpha/L^2. \tag{3}$$

This limited range of applicability (1) where the lumped-model formulation holds is graphically depicted in the unique thermal regime map of Fig. 2 by the shaded area shown in the Bi/Fo plane, where the horizontal and vertical coordinates are Fo and Bi, respectively.

Physically, the Bi number (2) represents the ratio of the internal heat-conduction resistance to the external convection resistance. Hence, a very large value of the Biot number (Bi >> 1) implies that *internal* thermal conduction is indeed very important in controlling the rate of heat transfer and therefore significant internal temperature variations will exist within the body. On the other hand, a very small value (Bi << 1) implies that the dominant thermal resistance is the *external* convection. This situation then will result in a relatively large temperature difference between the surface of the body and the cooling fluid compared with the internal temperature differences within the body itself, *i.e.* $(T_s - T_g) >> (T_{\max} - T_s)$. In other words, for problems possessing small Bi numbers the temperature differences inside the body are negligible compared with the outside temperature differences between the body and the cooling stream and hence will appear 'spatially uniform' in temperature.

The other coordinate, the Fourier number (3) can be regarded as dimensionless time or, preferably, the actual time normalized by the characteristic time for *pure conduction* $t_d = L^2/\alpha$. Unlike the Bi number, which has a *fixed* value for a given experiment, the value of the Fo number will *change* during the heating process from a small number at an early time (Fo << 1) to a large value (Fo >> 1) at very late times (*i.e.*

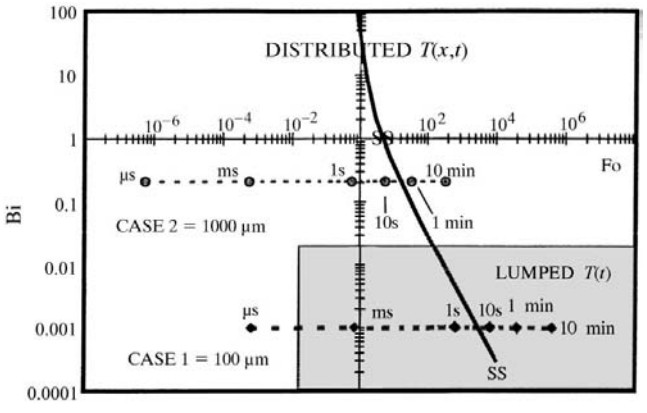


**Figure 2**
Thermal regime map, as a function of characteristic parameters, showing applicable regions of 'lumped' and 'distributed system' models.

**Table 1**
Nomenclature.

| | |
|---|---|
| $A$ | Surface area |
| Bi | Biot modulus |
| BC | Boundary conditions |
| $c$ | Specific heat |
| Fo | Fourier modulus |
| GE | Governing equation |
| $h$ | Convective heat-transfer film coefficient |
| IC | Initial condition |
| $k$ | Thermal conductivity |
| $L$ | Length (thickness of sample) |
| $m$ | Mass |
| $\dot{Q}$ | Total energy |
| $q''$ | Incident intensity of X-ray beam |
| $q'''$ | Volumetric internal heat generation |
| $R$ | Thermal resistance |
| $T$ | Temperature |
| $t$ | Time |
| $V$ | Volume |
| $x$ | Coordinate along beam direction |
| Subscripts/superscripts | |
| * | Non-dimensional quantity |
| att | Attenuation |
| cond | Conduction |
| conv | Convection |
| $i$ | Initial condition |
| sys | System |
| $\infty$ | Ambient, coolant |
| ss | Steady-state value |
| $s$ | Surface |
| $d$ | Diffusion time |
| Greek letters | |
| $\alpha$ | Thermal diffusivity |
| $\beta$ | Slope (Fig. 10) |
| $\delta$ | Absorption depth |
| $\lambda$ | Eigenvalue |
| $\Delta$ | Pulse length |
| $\xi$ | Non-dimensional $x$ |
| $\rho$ | Density |
| $\theta$ | Non-dimensional temperature |

traversing a horizontal line as the experiment proceeds). In an order-of-magnitude sense, the value of Fo = 1 denotes the system's characteristic (dimensionless) response time for pure thermal diffusion.

Hence, we see that the heat-transfer 'thermal regime map' (Fig. 2) serves two purposes: (i) it is used to show which model type the problem falls into once the actual value of the Bi is calculated for the given problem and (ii) it can be used to track and mark the transient evolution of the heat-transfer phenomenon, starting from the initial heating of the sample (Fo = 0) and continuing in time until the experiment ends. Relative to the internal heat diffusion time scale of the sample $t_d$, the process is divided into the 'very early' time (Fo << 1) in the heating process, before diffusion has adequate time to act, to the 'very late' time (Fo >> 1); that is, after sufficiently large time has passed and internal heat diffusion is complete. Diffusion in the intermediate time range ($0.02 < \mathrm{Fo} < 1$) leaves its signature varying in degree from having a small input to a very large impact.

Quick inspection of the thermal regime map in Fig. 2 shows that all problems, regardless of the value of the Biot number, initially behave as distributed systems for early times, $\mathrm{Fo} < 0.02$, because of the finite time it takes for thermal diffusion to take place. Only after the dimensionless time increases beyond $\mathrm{Fo} > 0.02$ will any change in the wall temperature be sensed throughout the body. (In fact, for $\mathrm{Fo} < 0.02$ the body actually behaves as though it was a semi-infinite solid, *i.e.* the center being totally unaware of any thermal changes occurring at the outer walls.) Thereafter, for times greater than $\mathrm{Fo} > 0.02$ the Biot number serves to discern if the bulk of the temperature difference is then experienced internally in the body (requiring distributed-model formulation) or externally (where the lumped-model approach can give reasonable values).

As time increases during the heating process, we expect the temperature of the body to eventually stabilize and ultimately reach thermal equilibrium with the external cooling fluid. The time required to achieve steady-state condition is also indicated on the thermal regime map. This is shown in Fig. 2 in terms of the amount of (dimensionless) time the process takes to cross the curved line (*i.e.* the solid line labeled as SS, steady state, shown traversing the figure from the very top center to the bottom right quadrant). Note that some discussion is required in order to fully explain how the exact position of the SS curved line was determined, but suffice it to say that it has been precisely located on this figure using classical heat-transfer theory. (Further details are provided in Appendix *A* for the interested reader.)

With the background material presented above, we are now in a position to thermally analyze the two specific test problems: specifically, a 100 µm thick cryocooled biocrystal and a 1000 µm thick air-cooled biocrystal. These 'thin' and 'thick' example problems will be thoroughly investigated in detail in the following section and are indicated in the thermal regime map by solid symbols, and are labeled as Case 1 and Case 2, respectively. In particular, from the thermal regime map one should first note that these two different test experiments are best described and analyzed by invoking the two different thermal models. The thin-sample case may be approximated as a lumped system, but the thick-sample problem must be solved as a distributed system. Secondly, the thermal regime map shows that significant internal thermal diffusion throughout the body (*i.e.* Fo = 1) takes just milliseconds in the thin-sample experiment but is of the order of seconds for the thick-sample case. Finally, we see from Fig. 2 that both test cases eventually reach steady state (as the dimensionless time increase from left to right and crosses the curved SS criteria line), but that this occurs very fast (in <10 s) for the thin-sample problem but takes substantially longer (∼60 s) for the thick sample. The detailed results of the thermal analyses that follow will be mostly reported in dimensional quantities but will often be cross-referenced and discussed in dimensionless terms to explain better the underlying thermophysics.

## 4. Lumped-model solutions

The resulting thermal behavior of the thin ($L$ = 100 µm) cryocooled biocrystal is shown in Fig. 3. For $h$ = 100 W m$^{-2}$ K$^{-1}$ (a reasonable estimate for the convective film coefficient for laminar gas-jet cooling) and taking $k$ = 5.0 W m$^{-1}$ K$^{-1}$ (thermal conductivity of vitrified ice), the Biot number therefore becomes Bi = 0.001 (based on the characteristic half thickness $L_c = L/2$). For such a small Biot number the lumped model is valid (equation 1; see Fig. 2). Neglecting internal spatial temperature gradients, the system energy balance reads

$$\rho c V \frac{\mathrm{d}T}{\mathrm{d}t} = q''' V - hA_S(T - T_\infty), \tag{4}$$

which physically represents the increase in thermal energy storage in the body owing to the absorption of X-rays (internal heat generation) less the convective heat loss. (All symbols used in the above lumped-model governing equation are defined in Table 1.) With $T = T_i = T_\infty$ at $t = 0$ initial condition, the temperature history of the thin sample is given by the simple expression

$$T(t) - T_\infty = \frac{q''' V}{hA_S}[1 - \exp(-t/t_{\mathrm{sys}})], \tag{5}$$

where

$$t_{\mathrm{sys}} = \rho C_p V/hA_S \tag{6}$$

is the representative (dimensional) system time constant for the lumped body, which depends on the ratio of the thermal capacitance of the system to the rate of convective heat transfer. Note that this characteristic time constant for the convectively cooled but spatially uniform lumped body, $t_{\mathrm{sys}}$, should not be confused with $t_d$, the representative time describing internal thermal diffusion defined earlier in connection with (3). Finally, note that quick inspection of the lumped solution (5) reveals that it takes three system time constants for the body to reach 95% of the final temperature.

The temperature rise as described by (5) is shown plotted in Fig. 3 for the pertinent physical and experimental parameters selected for our 'thin' sample problem. The beam intensity of $1 \times 10^{13}$ photons $s^{-1}$ $mm^{-2}$ at 8 keV striking a typical biosample having a beam attenuation length of $L_{att} = 1000$ µm results in 9.52% total absorption ($L^* = L/L_{att} = 0.1$), which translates to $\dot{q}'''V = q = 12.18$ µW in the above expression. Internal heat diffusion, by the definition of a lumped system, occurs so rapidly so as to eliminate all internal gradients within the sample (actually $t_d = 1.5$ ms) and the system time constant responding to external convection is $t_{sys} = 1.5$ s. As shown, the temperature of the sample rises quickly with time (see temperature history plot) and is always uniform throughout the sample (*i.e.* horizontal temperature profiles). In just 4.5 s (or three system time constants), the sample nears its steady-state final temperature, this being 6.09 K above the ambient gas temperature.

Neglecting convection altogether in the energy balance, *i.e.* eliminating the last term in (4), results in a totally different behavior for the temperature response. Now the temperature increases linearly with time as described by

$$T(t) = \frac{q'''V}{\rho c V} t + T_i, \qquad (7)$$

which is shown plotted in Fig. 4 assuming the same beam parameters and thermophysical properties as before. Without convective cooling, the solution predicts that the temperature will increase indefinitely without bounds at the constant rate of 4.1 K $s^{-1}$. This unrealistic prediction shows that convection is indeed the mechanism responsible for maintaining an acceptable sample temperature. Finally, the assumption of spatial uniformity is justified here owing to the small value of $L^* = 0.1$ (the beam's energy is deposited almost uniformly throughout the thickness of the sample) and the relatively short diffusion timescale (milliseconds for diffusion compared with the experimental time frame of seconds).

The importance of the convection is amplified further in Fig. 5(*a*), which shows the effect of the convective film coefficient on the resulting thermal behavior. A higher value of the convective coefficient ($h = 250$ W $m^{-2}$ $K^{-1}$) results in a substantially lower final steady-state temperature ($T_{ss} - T_\infty = 2.4$ K) and the required time taken to achieve steady state is also now reduced (note $t_{sys} = 0.6$ s; Table 2). The opposite is true as the value of the convection coefficient diminishes and at the limit, as $h$ goes to zero, the adiabatic solution is realised. As mentioned earlier, the exact true value of the convective film coefficient is somewhat uncertain (determination is rather complicated since its value depends on the fluid mechanics and gas properties), but as revealed by this figure its value has a substantial influence on the sample's temperature.

Next, for our estimated typical (and fixed) convection coefficient, the effect of the beam intensity on the temperature of the thin sample is illustrated in Fig. 5(*b*). As expected, as the intensity increases so does the temperature of the sample; increasing the photon flux by a factor of ten results in the same increase in final $\Delta T$ (steady-state temperature minus ambient) (Table 3). It is interesting to note that the system response time is unchanged, independent of source intensity, since the system time constant is fixed by the sample size, properties and heat-transfer coefficient (6).

The shape or more precisely the aspect ratio $V/A_s$ of the biocrystal is also known to be very important (Garman & Schneider, 1997; Garman, 1999) in determining the sample's temperature if one considers convection. Physically, smaller values of the $V/A_s$ ratio implies a larger surface area (relative to fixed volume) for convection, thus resulting in more cooling and hence lower temperatures. In this regard, long thin crystals are preferred over short thick crystals. This shape dependence is graphically illustrated by the plots reported in Fig. 5(*c*). Clearly, smaller values of $V/A_s$ result in substantially lower temperatures, as well as a faster response, as evidenced by the shorter time needed for the temperature to plateau (less time to steady state). Mathematically, note that this shape parameter appears twice in the solution to the spatially uniform thermal model (5), first explicitly as a multiplier in the coefficient dictating the magnitude of the temperature level and then again indirectly as part of the system time constant term $t_{sys}$, *i.e.* see (6), which controls the rate of the transient

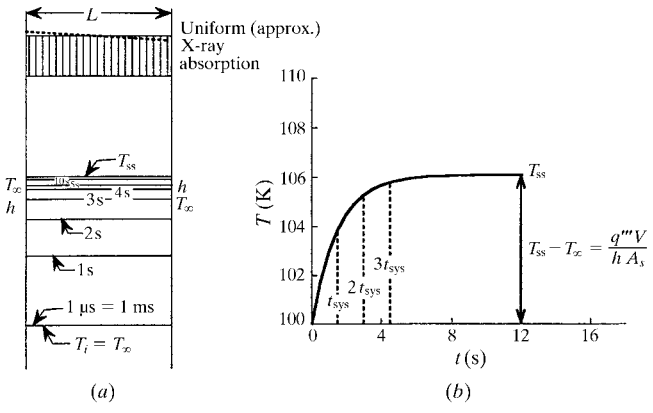


**Figure 3**
Thermal behavior of a thin cryocooled biocrystal. (*a*) Temperature profiles at selected times, (*b*) temperatures as a function of time.

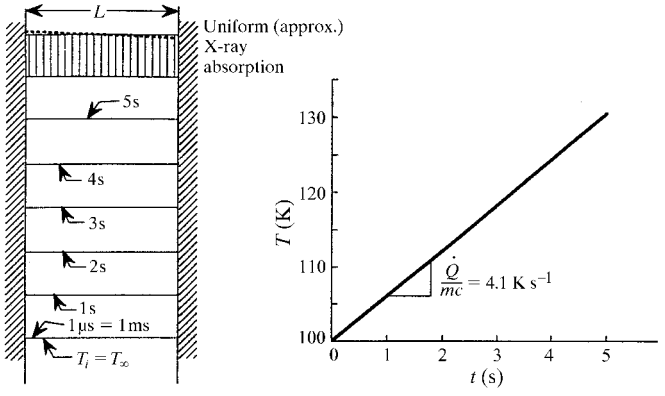


**Figure 4**
Thermal behavior of a thin insulated biocrystal at low temperature. (*a*) Temperature profiles at selected times, (*b*) temperatures as a function of time.

**Table 2**
Effect of corrective film coefficient.

| $h$ (W m$^{-2}$ K$^{-1}$) | $T_{ss} - T_{\infty}$ (K) | $t_{lumped}$ |
|---|---|---|
| 25 | 24.4 | 6.0 |
| 100 | 6.1 | 1.5 |
| 250 | 2.4 | 0.6 |

**Table 3**
Effect of beam intensity.

| $I_0$ (photons s$^{-1}$ mm$^{-2}$) | $T_{ss} - T_{\infty}$ (K) | $dT/dT\|_{t=0}$ (K s$^{-1}$) |
|---|---|---|
| $1 \times 10^{13}$ | 6.1 | 4.1 |
| $5 \times 10^{13}$ | 30.5 | 20.4 |
| $1 \times 10^{14}$ | 61 | 40.8 |

response. Finally note that this aspect-ratio shape dependence just described cannot be predicted if one invokes the adiabatic thermal model solution (7), *i.e.* the rate of the adiabatic temperature rise $dT/dt$ is independent of $V/A_s$ (see last column of Table 4).

In all of the examples discussed thus far, the beam, once initiated, was left on for a continuous period of time. To summarize, the system with convective cooling after $t > 3t_{sys}$ would stabilize at $T_{ss}$, but if the system was assumed adiabatic it would continue its linear ramp indefinitely. The response of the system after the beam is turned off for the two cases (convection and adiabatic boundary conditions, respectively) is shown in Fig. 6. With convection, the sample temperature, as expected, would fall back down to the gas-stream tempera-

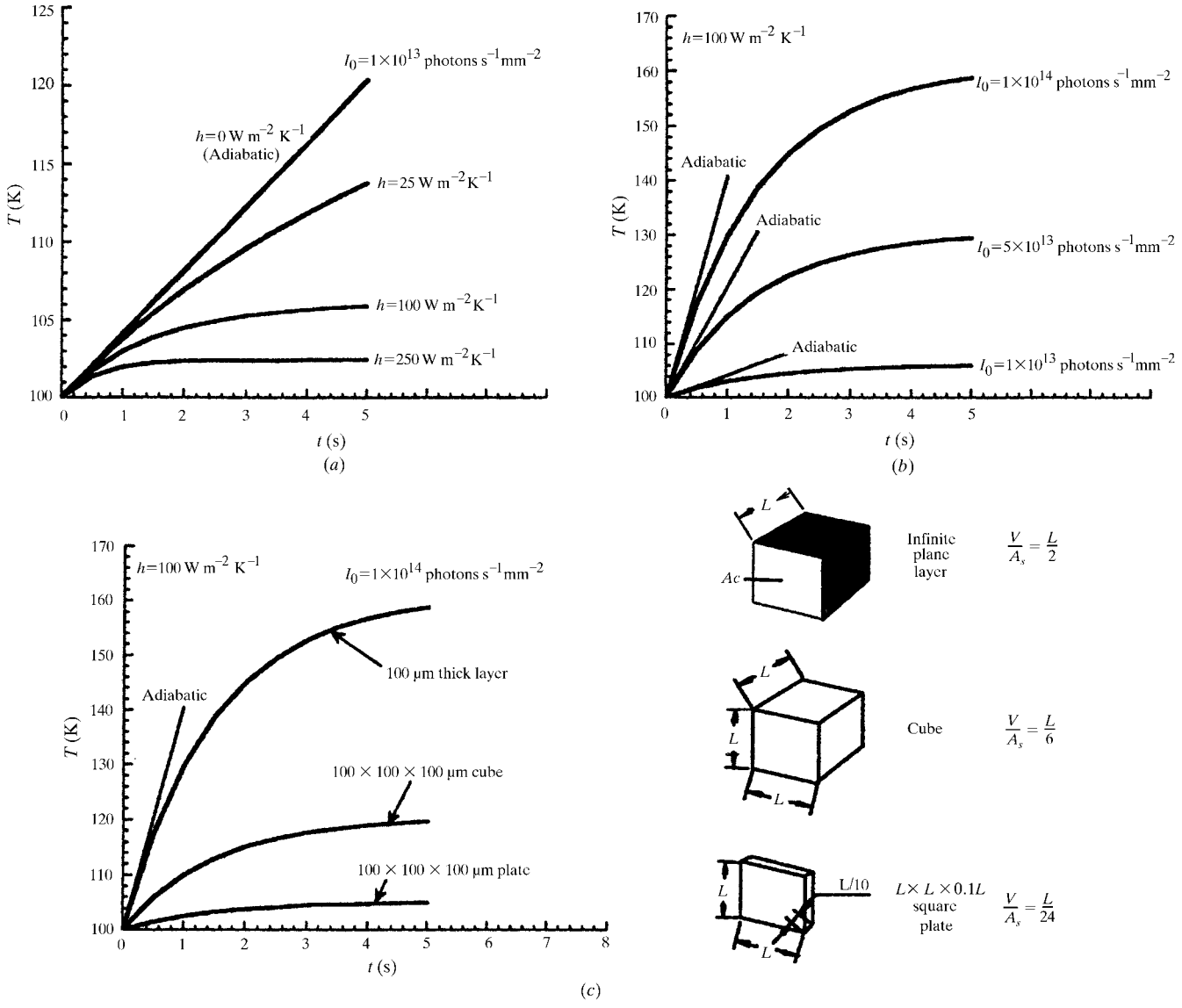


**Figure 5**
Thermal behavior of a thin cryocooled biocrystal showing (*a*) the effect of convective film coefficient, (*b*) beam intensity and (*c*) volume-to-surface area ratio.

**Table 4**
Effect of volume-to-surface area ratio.

| Shape | Dimensions (μm) | $V/A_s$ (μm) | Absorption (%)† | $T_{ss} - T_\infty$ (K) | $t_d$ (ms) | Bi | $t_{sys}$ (s) | $dT/dt\|_{t=0}$ (K s$^{-1}$) |
|---|---|---|---|---|---|---|---|---|
| Layer | $A_c$ 100 | 50 | 9.516 | 60.9 | 1.5 | 0.001 | 1.5 | 40.8 |
| Cube | 100 × 100 × 100 | 16.7 | 9.516 | 20.3 | 1.5 | 0.001 | 0.5 | 40.8 |
| Plate | 100 × 100 × 10 | 4.17 | 0.995 | 5.31 | 0.15 | 0.0001 | 0.125 | 42.63 |

† % X-rays absorbed = $[1 - \exp(-L/L_{att})]$; $dT/dt|_{t=0} = \dot{Q}_{abs}/\rho cV$.

ture, moreover, at precisely the same rate it took to heat up (same system time constant) following

$$T(t) - T_\infty = (T_{max} - T_\infty)\exp(-t/t_{sys}), \quad (8)$$

where $T_{max}$ is the last temperature experienced by the sample prior to beam deactivation. For the adiabatic case, in contrast, the temperature would remain constant after the removal of the heat source, fixed at its very latest value (*i.e.* generating horizontal temperature trace) since there is no 'thermal leakage' in the perfectly insulated system.

Let us focus for the moment on the lowest temperature curve plotted in Fig. 6 (with convection), which shows that after the beam is turned off the sample subsequently cools; however, the cooling process begins *before* the system has had enough time to reach a steady state. Here $\Delta t_p < t_{sys}$, resulting in $T_{max} - T_\infty = 2.97$ K (Table 5). For a much longer pulse duration (run 2, $\Delta t_p = 10$ s, where now $\Delta t_p > 3t_{sys}$), the system has plenty of time with respect to the system time constant to respond so that steady-state behavior prevails over the latter half of the pulse duration (run 2 of Table 5) and now $T(t) - T_\infty = 6.08$ K = constant. Thus, one concludes, as long as the pulse duration is 'sufficiently long' the temperature of the sample *at large time* (but before the beam is turned off) may be easily determined from

$$T_{ss} = T_\infty + \frac{q'''V}{hA_S} \quad \text{for } 3t_{sys} < t < \Delta t_p. \quad (9)$$

This maximum or steady-state temperature of the sample is obtained by taking the limit in (5) as $t$ becomes very large. (Note that if the above time restriction is not satisfied, the problem is always transient in nature.)

Another very interesting result is obtained from Table 5 by simultaneously comparing the plots of runs 2–5. Note that the total energy absorbed in all of these runs is the same. That is, the sample is exposed to exactly the same number of photons, namely $1 \times 10^{12}$ photons, but over a shorter and shorter time period. (Here, we take the frontal cross-sectional area of the biocrystal to be $A_c = 0.1 \times 0.1$ mm.) A comparison of the plots reveals that keeping the total thermal loading the same but experienced over a shorter and shorter time period results in a significantly elevated maximum sample temperature: for example, the sample temperature increases from $\Delta T_{max} = 6.08$ K, if distributed evenly over the 10 s interval, to as high as 39.44 K, provided the total amount of energy is delivered very quickly in only 0.1 s. This difference in $T_{max}$ is attributed, of course, to the higher flux level, but note however that an accurate value for $T_{max}$ can only be predicted when convective cooling is included. The adiabatic model, on the other hand, always predicts the same final maximum temperature as long as the total thermal load is the same.

As the $\Delta t$ pulse duration decreases (*i.e.* less time for convection), we see that the adiabatic model and the convective thermal model predictions clearly approach one another until finally the two solutions produce essentially the same result (compare the adiabatic model and convection results, run 5, during heating in which $\Delta t_p = 0.1 << t_{sys}$), but disagree totally thereafter during the cooling phase. This is explained as a result of the finite time required for convection to be felt (again, of the order of the $t_{sys} = 1.5$ s).

Extending this last conclusion (*i.e.* convection and adiabatic results are identical over very short times) to an even shorter pulse duration is the basis for the calculation used to produce Fig. 7. Here again the same number of photons ($1 \times 10^{12}$) strikes the sample as before, but now in just 100 fs. The calculation here is very straightforward, is now based upon the adiabatic thermal model and produces the result as indicated. The advantage here in dealing with this extremely short time is that convection can truly be eliminated from the model (over both the heating event as well as during the 'short time' cooling period). The major problem, however, is that the solution itself becomes *null and void* since the governing equation used to generate this solution breaks down for such a short time interval (Ozisik & Tzou, 1994). Thermal analysis of this thin sample in this ultrashort time domain requires a new and more refined mathematical formulation to describe the thermal energy transport (Kuzay & Kazmierczak, 2001); accurate and reliable solutions applicable to this time range are the subject of ongoing research. Suffice it to say that the impetus driving the inquiry into X-ray/biomaterial interaction at this ultrashort femtosecond timescale is the future X-ray free-electron laser (FEL) light source and its exciting new applications. Hence, the solution we report as Fig. 7, albeit

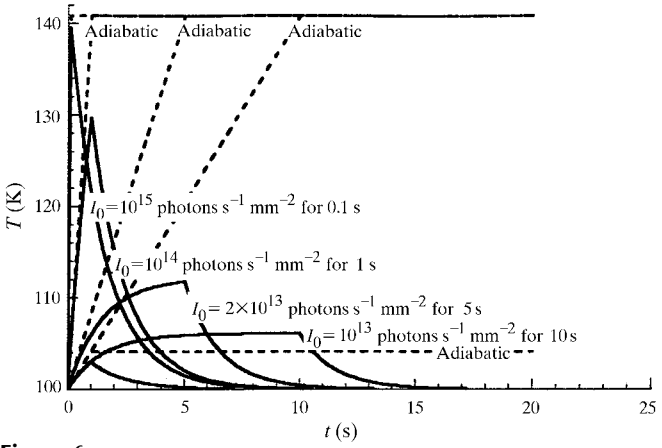


**Figure 6**
Thermal behavior of a thin cryocooled sample showing the effect of a single pulse of decreasing duration (but fixed total load).

**Table 5**
Effect of finite pulse duration.

$dT/dt|_{t=0} = \dot{Q}_{Abs}/\rho Cv$; $T_{Adia} - T_i = \dot{Q}_{Abs}\Delta t_p/\rho Cv = 40.77$ K.

| $I_0$ (photons s$^{-1}$ mm$^2$) | $\Delta t_p$ (s) | $I_0 A_c \Delta t$ (photons) | $dT/dt\|_{t=0}$ | $T_{max} - T_\infty$ (K) |
|---|---|---|---|---|
| $1 \times 10^{13}$ | 1 | $1 \times 10^{11}$ | 4.08 | 2.97 |
| $1 \times 10^{13}$ | 10 | $1 \times 10^{12}$ | 4.08 | 6.08 |
| $2 \times 10^{13}$ | 5 | $1 \times 10^{12}$ | 8.15 | 11.75 |
| $1 \times 10^{14}$ | 1 | $1 \times 10^{12}$ | 40.77 | 29.72 |
| $1 \times 10^{15}$ | 0.1 | $1 \times 10^{12}$ | 407.74 | 39.44 |

totally erroneous, is presented here mainly for future comparison.

## 5. Distributed-model solutions

Suppose now the thickness of the selected crystal is much larger and $L = 1000$ µm. The increased depth will result in two very significant changes: (i) greater X-ray absorption and (ii) spatial dependence.

In reference to the first concern, the ratio of the sample thickness $L$ to the attenuation length of X-ray beam $L_{att}$ in this case is now $L/L_{att} = L^* = 1$. Therefore, 63.2% of the energy striking the sample is now absorbed as it passes through the sample compared with just 9.52% for the 100 µm thick sample. This greater absorption implies more internal heating and therefore higher sample temperatures, but may also simultaneously impose significant non-uniformity in the heat-source distribution. Unlike the thin-sample model, in which the internal heat generation may be reasonably approximated as uniform over the sample's depth, the *local* variation in heat absorption (*i.e.* the exponential decay in space) through the sample must now be considered. Also note that this added thickness results in additional internal thermal resistance; the absorbed energy must be conducted a longer distance before it can be convected away by the external cooling stream. Recall that the two thermal resistances, as explained earlier, are brought into perspective relative to each other in terms of the dimensionless Biot number. For this thick biocrystal, the Biot number is significantly larger, Bi = 0.208, and now one finds that, as per the thermal regime map (Fig. 2), this necessitates solving the distributed thermal model in order to obtain an accurate solution. For transient one-dimensional heat conduction with exponential decay in internal heat absorption (in the $x$ direction), the applicable governing equation to solve is now

$$\frac{\partial^2 T}{\partial x^2} + \frac{q''/\delta}{k}\exp(-x/\delta) = (1/\alpha)\frac{\partial T}{\partial t}, \tag{10}$$

subjected to the convective boundary conditions, formally stated as

$$\begin{aligned} -k\frac{\partial T}{\partial x}(0,t) &= h[T_\infty - T(0,t)] \\ -k\frac{\partial T}{\partial x}(L,t) &= h[T(L,t) - T_\infty]. \end{aligned} \tag{11}$$

For the imposed initial condition $T = T_i = T_\infty$ at $t = 0$, this system of equations is readily solved using the method of separation of variables (Ozisik, 1993) rendering the following expression for the temperature distribution

$$\begin{aligned} T(x,t) - T_\infty = [T_{ss}(x) - T_\infty] - \frac{q''L}{k} \\ \times \sum_{n=1,2,3}^{\infty} \frac{\Phi(\lambda_n, x/L)}{N_n(\lambda_n)L}\exp(-\lambda_n^2 \alpha t/L^2) \\ \times \int_0^L [T_{ss}(x) - T_\infty]\Phi(\lambda_n, x/L)\,dx \end{aligned} \tag{12}$$

in which

$$\begin{aligned} T_{ss}(x) - T_\infty = \frac{q''L}{k}\left\{ \frac{-\delta}{L}\exp(-x/\delta) \right. \\ + \frac{(h\delta/k)[\exp(-L/\delta) - 1] - [\exp(-L/\delta) + 1]}{2 + hL/k} \\ \left. \times \left(\frac{x}{L} + \frac{k}{hL}\right) + \frac{k}{hL} + \frac{\delta}{L}\right\}, \end{aligned} \tag{13}$$

where the eigenfunction and normalization integral in (12) are

$$\Phi(\lambda_n, x/L) = \lambda_n \cos(\lambda_n x/L) + (hL/k)\sin(\lambda_n x/L), \tag{14}$$

$$\begin{aligned} N_n(\lambda) &= \frac{1}{L}\int_0^L \Phi^2(\lambda_n, x/L)\,dx \\ &= \frac{1}{2}\left\{\left[\lambda_n^2 + \left(\frac{hL}{k}\right)^2\right]\left[1 + \frac{hL/k}{\lambda_n^2 + (hL/k)^2}\right] + \frac{hL}{k}\right\} \end{aligned} \tag{15}$$

and where the eigenvalues $\lambda_n$ are determined from the eigencondition

$$2\cot\lambda_n = \left(\frac{\lambda_n}{hL/k} - \frac{hL/k}{\lambda_n}\right). \tag{16}$$

In evaluating this solution, we assumed that the sample is exposed to the same 'typical' beam intensity of $1 \times 10^{13}$ photons s$^{-1}$ mm$^{-2}$ at 8 keV as before. With the beam attenuation length of 1000 µm, $L^* = 1.0$ or 63.2% absorption; this now creates the total of 80.91 µW to be generated within

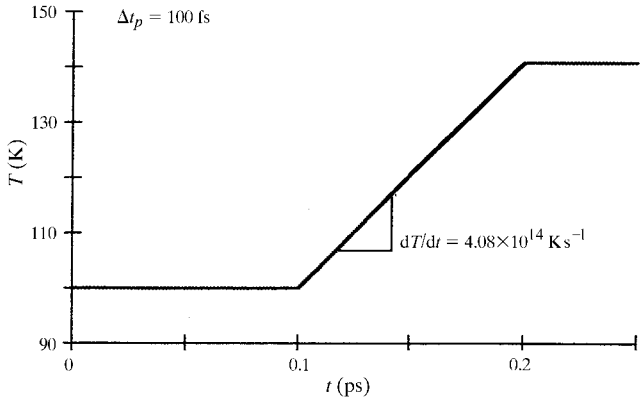


**Figure 7**
Erroneous calculation showing the thermal behavior of a thin biocrystal for extreme heat flux over an ultrashort time using the classical (adiabatic) heat-transfer model for step source variation.

the sample but moreover is distributed non-uniformly throughout the sample with an exponentially decaying spatial variation. Note that the thermal properties used in analyzing this 'thick-case' problem are that of water at room temperature ($k$ = 0.6 W m$^{-1}$ K$^{-1}$); also, the high heat-transfer coefficient $h$ = 250 W m$^{-2}$ K$^{-1}$ was assumed. This selection of a lower $k$ than in the cryocooled case and a higher heat-transfer coefficient was made mainly to accentuate the spatial gradients effects associated with higher Bi numbers.

The thermal response of the thick ($L$ = 1000 µm) air-cooled biocrystal is plotted in Fig. 8. Just like the lumped-system model, the temperature of the sample increases rapidly at first, then slows and then eventually becomes steady with time when the internal heat generation and the rate of convective heat loss become equal. According to the temperature traces, the time it takes to achieve steady-state conditions for the thick layer is about 60 s compared with just 1.8 s for the thin sample (Fig. 5*a*, high $h$ case). (In terms of the dimensionless regime map, Fig. 2, the Fourier number, given Bi = 0.208, needs to be greater than Fo = 30 to achieve steady-state conditions or $t$ = 52 s, since $t_d = L^2/\alpha$ = 1.736 s.) This is much longer owing to the larger volume and to the additional internal conductive resistance to overcome. The most striking difference between the lumped and distributed solutions are the temperature profiles ($T$ *versus* $x$ at select times), which clearly display the spatial dependence now allowed in the solution. Hence one sees, at any given instant of time, the appearance of a peak temperature initially located near the left wall which then travels toward the center of the sample as time increases. Owing to the non-uniform heating (*i.e.* exponential decay in absorption), however, note that the location of the maximum temperature under steady-state conditions remains slightly off-center (slightly left of the centerline). Moving away from $T_{max}$, the temperature then smoothly decreases towards the walls where the convective cooling is felt. Under these experimental conditions, the sample's final sustained peak temperature is $T_{max} - T_\infty$ = 17.94 K (as opposed to 2.44 K for the thin sample) and the final (steady-state) largest internal temperature difference is $T_{max} - T(L)$ = 2.19 K.

For the sake of completeness, the distributed model for the thick sample but for the case of *insulated outer walls* is reported in Fig. 9. This solution involves the same governing equation (10) but the convective BC (11) is replaced with $dT/dx = 0$ at $x = 0 = L$. An exact analytical solution is again possible using the method of separation of variables, which results in the following expression

$$T(x,t) - T_i = \frac{q''/L}{k}\left\{1 - \exp(L/\delta)\frac{t\alpha}{L^2} + \sum_{n=1,2,3}^{\infty}\frac{2(L/\delta)^2}{(L/\delta)^2 + n^2\pi^2}[1-(-1)^n\exp(-x/\delta)] \times \left[\frac{1}{n^2\pi^2} - \frac{\exp(-n^2\pi^2 t\alpha/L^2)}{n^2\pi^2}\right]\cos(n\pi x/L)\right\}. \quad (17)$$

This solution is evaluated (for the same beam conditions as used in Fig. 8) and produces the representative temperature profiles and thermal traces shown in Fig. 9. Here, we see that the temperature of the sample, without taking into account the benefit of convective cooling, will increase with time indefinitely. This is exactly analogous to the results presented in Fig. 4 for the lumped model, except now the internal heat conduction is included in the thermal model (*via* the second-order space derivative term). The exponentially decreasing energy absorption causes the temperature near the front surface of the sample to always be higher in magnitude than the rear, which eventually reaches (and stabilizes) at around $\Delta T \simeq 1$ K after the 'early time' transient adjustment period, depicted by the *spatially* changing temperature profiles, dies out. Thereafter, the temperatures at all locations 'after suffi-

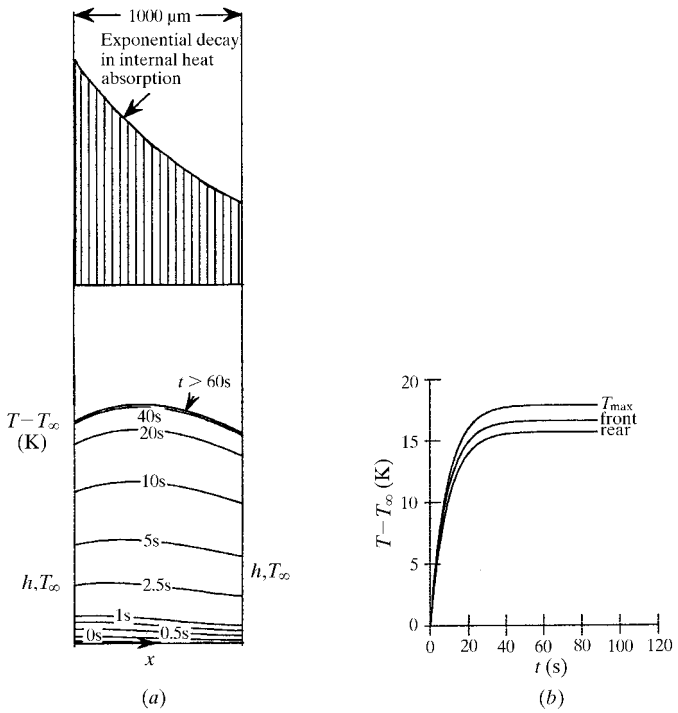


**Figure 8**
Thermal behavior of a thick air-cooled biocrystal. (*a*) Temperature profiles at selected times, (*b*) temperature histories at selected locations.

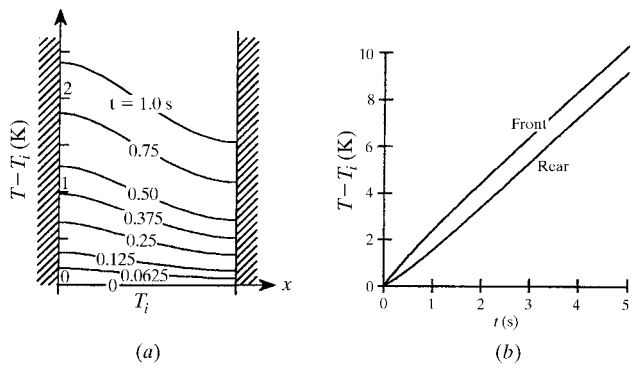


**Figure 9**
Thermal behavior of a thick insulated biocrystal. (*a*) Temperature profiles at selected times, (*b*) temperature histories at selected locations.

ciently large time' increase linearly with time. (The meaning of sufficiently large time, clearly, is with reference to the pure diffusion time scale of the system, namely $t_d$ = 1.736 s, since convection is not present.) It is interesting to note that although the thick sample is absorbing energy at more than six times the rate of the thin sample (*i.e.* 63.21 *versus* 9.52%), the adiabatic temperature rise of the thick sample at large time is actually less (1.9 K $s^{-1}$ *versus* 4.1 K $s^{-1}$) owing to the tenfold larger volume and the different thermophysical properties. Finally, again we wish to emphasize that this adiabatic model and solutions are *not* physically correct (except for extremely short times, as explained earlier in connection with Figs. 6 and 7), but are presented here for completeness. In order to realistically model the thermal behavior of the thick-layer system over the time domain encountered in typical crystallography experiments, the thermal analysis *must* include convection.

Now having firmly established the fact that convection plays an indispensable role in determining the temperature distribution of the sample once again, let us explore the effect of the absorption distribution *variation* within the sample. Taking the thick sample, $L$ = 1000 µm, as the test case, we alter the assumed absorption variation in the distributed model from the correct exponential decay (curve $A$, Fig. 10$a$), to two linear approximations (lines $B$ and $C$, both very reasonable fits but involving different endpoints) and finally to the totally incorrect uniform (line $D$) absorption distribution. Solving the distributed model with these four different internal heat-generation variations and focusing at large time only results in the steady-state temperature profiles depicted in Fig. 10($b$). Approximating the exponential variation with a linear fit produces the correct overall shape (parabolic with slight asymmetry). However, it overpredicts the magnitude of the temperature if the linear fit assumed the same endpoints (profile $B$) as the exponential decay (owing to higher total input power), but fits the correct solution (profile $A$) almost exactly (*i.e.* generates the same profile within the plotting resolution used in the figure) if the linear fit was constrained so as to give the same total power (profile $C$). The wildly inaccurate uniform distribution (with same total power), profile $D$, deviates from the exact result in being perfectly symmetric about the centerline but gives nearly the same peak temperature. Finally, note that the steady-state profiles themselves become totally independent of the type of the internal heat-generation variation if the internal heat-conduction resistance is neglected altogether (*i.e.* lumped-model solution) resulting in the very bottom 'flat' profile. Examining the difference between the correct temperature solution (profile $A$ based upon exponential decay) with the lumped-model solution (*i.e.* the horizontal line) clearly reveals the resulting consequence and the extent of the error (at large time) attributed to the lumped-model simplification (*i.e.* negligible spatial dependence) for the case of $L^*$ = 1.

It is also instructive to investigate the effect of the attenuation length $L_{att}$ on the resulting steady-state temperature profile within the thick-layer problem. Here, the thickness of the sample and the external film coefficient are set to $L$ = 1000 µm and $h$ = 250 W $m^{-2}$ $K^{-1}$, respectively, and $L_{att}$ is varied. The actual value of $L_{att}$, of course, depends on the photon's energy level (*i.e.* keV) and on the type of material being investigated, but for illustrative purposes $L_{att}$ is varied as 50, 1000 and 10 000 µm. (Note that earlier $L_{att}$ was set at 1000 µm for both the thin and thick test problems, since the same beam energy level and material type were assumed.) The final steady-state temperature profile with exponential decay in absorption (hence, the correct internal heat-generation variation is used without any approximation in the remaining figure) is described (in dimensionless form) by

$$\Theta(\xi) = \frac{-\exp(-\xi L^*)}{L^*} + \frac{(B_i/L^*)[\exp(-L^*) - 1] - [\exp(-L^*) + 1]}{2 + B_i}\left(\xi + \frac{1}{B_i}\right) + \frac{1}{B_i} + \frac{1}{L^*}, \quad (18)$$

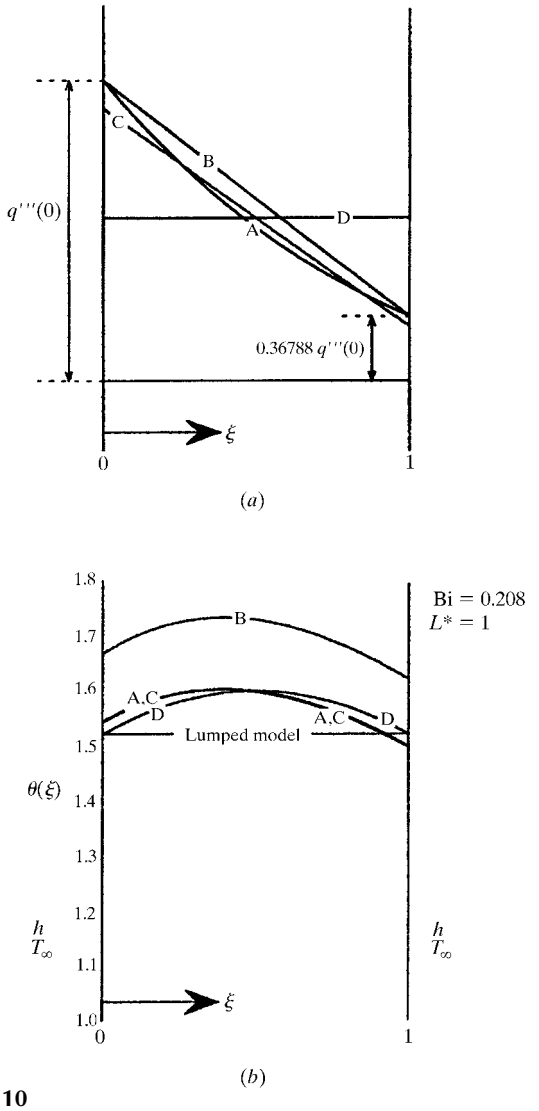


**Figure 10**
Effect of absorption distribution approximation on steady-state temperature profile for $L^*$ = 1 and Bi = 0.208. ($a$) Assumed variation in heat absorption, ($b$) resulting steady-state temperature profile.

where the dimensionless variables are defined as follows

$$\Theta = T - T_\infty/(q'' L/k);\ \xi = x/L;\ L^* = L/L_{\rm att};\ B_i = hL/k. \tag{19}$$

The above expression can be obtained by taking the limit as $t$ goes to infinity in the distributed solution (12) or by directly solving the governing equation (10) with the time-derivative term set equal to zero. The above solution (18) plotted for the selected values of $L^* = 20$, 1 and 0.1 is shown in Fig. 11(*a*). The case of $L^* = 1$ ($L_{\rm att} = 1000\ \mu$m), featuring a parabolic temperature profile with slight asymmetry, *i.e.* peak temperature shifted slightly toward the left owing to the non-uniform exponential heating, was thoroughly discussed earlier in connection with the solution at large time of Fig. 8. The resulting final temperature profile for the system having a much shorter attenuation length $L_{\rm att} = 50$ ($L^* = 20$) is very different. The peak temperature now occurs near the far left wall and the temperature then drops in a linear fashion through the remaining thickness. Note also that the magnitude of the temperature is significantly higher for $L^* = 20$ *versus* $L^* = 1$ owing to the much greater total absorption (*i.e.* now 100 *versus* 63.2%). Finally note that, if (18) was plotted for *higher* values of $L^* > 20$ (or $L_{\rm att} < 50\ \mu$m), all of the profiles generated in that case (not shown) would essentially look the same as the result of the $L^* = 20$ case since all of the energy absorbed would be deposited in nearly the same manner in the very thin front surface region. Finally, consider the other extreme value; here, one observes that for the case with the very longest attenuation length $L_{\rm att} = 10\,000\ \mu$m (or $L^* = 0.1$), the steady-state temperature profile tends to appear almost flat (with just a slight peak at the centerline) and is least in value. The low magnitude is readily explained: under this condition, most of the energy of the X-ray beam passes right through (just 9.52% of the total energy is absorbed; the same as in the thin-sample study) and moreover note that of the energy that is absorbed, it is more or less evenly distributed throughout the layer (and hence the maximum temperature occurs at the center).

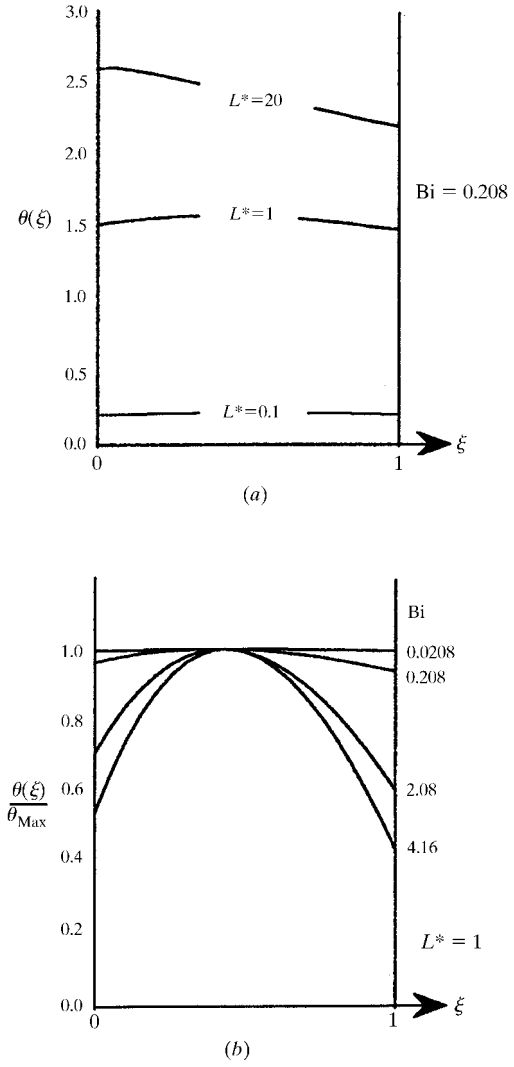


**Figure 11**
Effect of (*a*) $L^*$ and (*b*) Bi number on steady-state temperature profile for the distributed model with exponential heat absorption.

Finally, the steady-state temperature solution given by (18) is parametrically exercised one last time, this time fixing the dimensionless attenuation length to $L^* = 1$ (typical value for the thick-sample problem) and the other dimensionless parameter, the Bi number, in the expression is allowed to change. Recall that the value of the Bi number can be thought of as the dimensionless heat-transfer coefficient (the relative strength of the convective cooling, keeping $L$ and $k$ constant), or preferably as the ratio of the internal conduction resistance to the external convection resistance. From the plots shown in Fig. 11(*b*), one observes that as the Bi number increases the temperature difference *within* the sample also increases (that is, relative to the overall temperature difference $\Delta T_{\rm max} = T_{\rm max} - T_\infty$, which includes both internal conduction and outer convective temperature drops). For example, for Bi = 0.208 (thick layer test problem), between 5 and 10% of the total $\Delta T$ occurs within the sample but now accounts for greater than 40% (55%) for Bi = 2.08 (4.16). This behavior is perfectly consistent with the physical interpretations and understanding of Bi number described above. On the other hand, decreasing the value of the Biot number by a factor of ten down to Bi = 0.0208 results in smaller (relative) internal spatial gradients and therefore 'flatter' temperature profiles (see the very top profile in Fig. 11*b*). It is important to point out that this last example just presented provides direct quantitative justification for the range of validity of the lumped-model assumption expressed earlier, *i.e.* as clearly illustrated a distributed system essentially behaves and thus can be effectively modeled as a lumped body provided Bi < 0.02 as delineated in the thermal regime map in Fig. 2.

## 6. Conclusions

In this paper, the thermal problem associated with the X-ray beam and biomaterial interaction has been comprehensively analyzed for the third-generation synchrotron sources. All interactions can be treated using conventional heat-transfer formulation. A unique regime map using Fo and Bi as the running parameters has been developed to identify the

particular mathematical model (lumped or distributed system) that should be used along with quantitative criteria that allows one to check for the steady-state condition. Within this framework, thin- and thick-sample test cases were carefully studied and the resulting thermal response, *i.e.* temperature distributions as function of time and position, subjected to a realistic third-generation beam of 8 keV photon energy and at typical flux levels of $10^{13}$ photons $mm^{-2}$ $s^{-1}$ were reported in detail. For this set of beam parameters the heat-transfer analysis revealed that the temperature of the thin (100 μm thick) cryocooled crystal will increase 6 K and would take just 4.5 s to stabilize, whereas the 1 mm thick crystal will take more than 52 s of constant X-ray exposure before achieving steady state and the temperature would reach 18 K above the ambient. Moreover, it was shown that the temperature would vary significantly *across* the thick crystal (as much as 2 K), whereas the temperature gradients within the thin sample were negligible (*i.e.* a nearly isothermal crystal).

For the benefit of the researchers dealing with cryocooled biosamples and interested in calculating its temperature level during X-ray exposure, the two types of generalized heat-transfer solutions were presented in detail. It was shown that provided certain conditions are satisfied (*i.e.* Bi < 0.02 and $F_o > 0.02$) the simplified lumped-model solutions are applicable, the results of which will be very close to the true solution. The very simple lumped-model solution revealed and explained many interesting trends, such as the strong influence that convection has on the final temperature (and on the rate of temperature change) and the importance of the volume-to-surface area ratio. It also provided the characteristic thermal time constant of the system $t_{sys} = \rho C_p V/hA_S$; by evaluating this simple expression for $t_{sys}$ ($\times$ 3) experimenters now know how long heating and cooling of very small (nearly isothermal) crystals take.

More refined distributed model solutions were also developed that took into account internal heat conduction and spatial dependence and plots were generated that showed the resulting internal temperature gradients in detail. The extent of the accompanying elevated internal temperatures was revealed over a large range of the $L^*$ and Bi parameters (at steady state), allowing the users to decide if the additional effort and mathematics needed is warranted. The transient response of the distributed system now also depends on the rate of internal thermal diffusion. The characteristic timescale for pure thermal diffusion can be estimated in an order-of-magnitude sense by $t_d \simeq L^2/\alpha$ or Fo = 1. Hence, the overall *system* time constant for the convectively cooled body with internal conduction is thus more involved than the lumped body; the time it takes for a distributed system to reach steady state is therefore more complicated to express and was given in graphical form (*i.e.* curved SS line) in Fig. 2. It was also revealed that it is the amount of energy deposited and not necessarily so much the exact distribution of the internal thermal energy source within the sample that dictates the maximum temperature.

Finally, irrespective of whether the lumped- or the distributed-model solutions are ultimately used, it was clearly shown that *convection* should always be considered as part of the analysis at all times (except for extremely short time periods), although it is noted that the lack of accurate information for the convective film coefficient can be a major source of uncertainty in the thermal analysis. For completeness and to further emphasize the role of convection, the results of both convective thermal models were also compared with the results generated assuming the adiabatic thermal model, the typical formulation used in all earlier thermal heating studies.

Overall, the results reported herein have provided a much better and true understanding of the expected thermal behavior of biocrystals during X-ray heating under a range of conditions. In closing, we wish to leave the reader with some general guidelines to help reduce crystal heating during X-ray exposure. From a pure thermal engineering perspective and assuming that the beam-energy/flux level of the experiment cannot change, three simple and obvious recommendations that come to mind supported by this work are as follows: (i) the thinner the crystal the better, (ii) crystals shapes that possess higher values of volume-to-surface area ratio are preferred and (iii) always adjust the cooling-gas flow rate to provide the highest possible overall heat-transfer film coefficient. The exact impact of each of these suggestions has been thoroughly quantified during the course of this investigation and has been shown to be quite dramatic; implementation of any one strategy could easily cut the total temperature increase in the sample at least in half. Also note that it is possible to reduce the maximum temperature of the sample by carefully adjusting the length of time that the X-ray beam is on. Specifically, if the X-ray exposure duration is made much shorter than the time it takes for the system to reach thermal equilibrium, then the temperature of the sample will be less than the maximum steady-state value $T_{ss}$ (provided one allows sufficient time for cooling down between the multiple heating cycles throughout the entire data-collection process). On the other hand, note that exposing the sample to much longer X-ray exposure times will *not* result in further temperature increase beyond $T_{ss}$, which is directly opposite to our prior understanding of the thermal behavior based upon the earlier adiabatic thermal model. Lastly, we hope that this study has adequately equipped the users with enough knowledge in thermal analysis and modeling capabilities tools so as to allow the users themselves to easily and accurately calculate the temperature increases during other experiments run under different conditions.

## APPENDIX *A*

The exact position of the solid SS curved line (denoting the minimum dimensionless time the experiment requires for the system to attain steady state) has been precisely located using classical heat-transfer theory. In short, it was generated by smoothly fitting a line through the steady-state criteria applicable to three different transient convective heat-transfer problem types, each valid for a different range of Bi numbers;

namely: (i) those having extremely large Biot numbers, Bi $\rightarrow \infty$, (ii) those with very small Biot numbers, Bi $< 0.02$, and (iii) the class of problem having Bi numbers somewhere in between, $0.02 <$ Bi $< 100$ (*i.e.* moderate values of Bi numbers).

For pure *conduction-limited* (*i.e.* Bi $\rightarrow \infty$) but convectively cooled heat-transfer problems, it can be shown using the theoretical solutions to the distributed plane layer problem (Bejan, 1993; Ozisik, 1993) for which $h \rightarrow \infty$ (*i.e.* a case of sudden change in wall temperature) that the system nears steady state (about 98% of final values) at about Fo = 0.5. Thus, the criterion indicating the occurrence of the steady-state condition for very high Bi number problems is as follows,

$$\text{if Fo} > 0.5 \text{ then the system is at SS for Bi} \rightarrow \infty. \quad (20)$$

(20) serves as the upper asymptote of the curved SS line plotted in Fig. 2 (*i.e.* vertical line at Fo = 0.5, located above the top of the plot). Again it is important to emphasize that this steady-state criterion described above applies only to systems where the cooling is restricted/limited by the rate of internal heat conduction only, *i.e.* Bi $\rightarrow \infty$, and hence the extent of the transient cooling or the degree to which the system nears steady-state is indicated (in terms of the non-dimensional time) by the magnitude of the Fo number, the (dimensionless) heat-diffusion time scale.

With regards to problem category (ii) above, those with very small Biot numbers (Bi $< 0.02$) or lumped-type behavior, that is for convectively cooled system *with negligible internal resistance*, the applicable steady-state criterion is totally different. Instead, the steady-state criterion now reads

$$\text{if BiFo} > 3, \text{ then the system is at SS for Bi} < 0.02. \quad (21)$$

The above criterion (21) is easily derived from the fact that the solution for the temperature, assuming the lumped model, takes three system time constants for the body to reach 95% of the final temperature. (21) serves as the lower asymptote for the curved SS criterion line (*i.e.* straight line defined by Bi = 3/Fo located in the lower right-hand quadrant or the lumped-body region of Fig. 2). Note here for this *convection-controlled* system that it can be shown that the dimensionless parameter BiFo physically represents the ratio of the rate of convective heat transfer to the rate of sensible thermal energy storage. Thus here, for this case the rate of cooling/heating of the system depends entirely on the rate of convection (and amount of sensible thermal energy storage) and the internal heat conduction is so large by comparison that it plays no role, relatively speaking, in determining the thermal history of the sample.

Finally, the time required for the system to effectively reach a steady state for moderate values of the Bi number ($0.02 <$ Bi $< 100$), the region located between the two extremes just specified (*i.e.* conduction-limited, convection-controlled cooling), is a little more complicated than the two limiting cases since the overall system time response now depends on *both* the rate of internal heat diffusion (characterized by Fo) *and* also on the rate of convection coupled to the thermal capacitance of the system, *i.e.* FoBi. The criterion that indicates the minimum dimensionless time needed to reach steady state for this range of Bi is graphically represented in Fig. 2 by the curved line bridging the two limits (20) and (21), respectively. This curve was generated by carefully evaluating the theoretical (distributed model) solutions for the given range of Bi numbers using the criteria that the centerline temperature of system attains at least 90% of its final value and by allowing the endpoints of this curve to smoothly join the two stated limits. Functionally, one observes from Fig. 2 that the resultant curve (denoting the point in dimensionless time where steady-state behavior ensues) for this Bi number range depends on both the Fo and Bi numbers in a non-linear fashion.

This work was partially supported by the US Department of Energy, Office of Science under Contract No. W-31-109-Eng-38.

## References

Anfinrud, P. A. (1999). Private communication.
Bejan, A. (1993). *Heat Transfer*, p. 153. New York: John Wiley & Sons, Inc.
Blake, C. C. F. & Phillips, D. C. (1962). *Biological Effects of Ionizing Radiation at the Molecular Level*, AAEA Symposium, Vienna, p. 183.
Garman, E. F. (1999). *Acta Cryst.* D**55**, 1641–1653.
Garman, E. F. & Schneider, T. R. (1997). *J. Appl. Cryst.* **30**, 211–237.
Gonzalez, A. & Nave, C. (1994). *Acta Cryst.* D**50**, 874–877.
Helliwell, J. R. (1992). *Macromolecular Crystallography with Synchrotron Radiation.* Cambridge University Press.
Hope, H., Frolow, F., von Böhlen, K., Makowski, I., Kratky, C., Halfon, Y., Danz, H., Webster, P., Bartels, K. S., Wittmann, H. G. & Yonath, A. (1989). *Acta Cryst.* B**45**, 190–199.
Kuzay, T. M. & Kazmierczak, M. (2001). *J. Synchrotron Rad.* Submitted.
Lock, G. S. H. (1990). *The Growth and Decay of Ice*, pp. 302–329. Cambridge University Press.
Nave, C. (1995). *Radiat. Phys. Chem.* **45**, 483–490.
Ozisik, M. N. (1993). *Heat Conduction.* New York: John Wiley & Sons, Inc.
Ozisik, M. N. & Tzou, D. Y. (1994). *J. Heat Transfer*, **116**, 526–535.
Ren, Z., Bourgeois, D., Helliwell, J. R., Moffat, K., Srajer, V. & Stoddard, B. L. (1999). *J. Synchrotron Rad.* **6**, 891–917.
Srajer, V., Teng, T.-Y., Ursby, T., Pradervand, C., Ren, Z., Adachi, S.-I., Schildkamp, W., Bourgeois, D, Wulff, M. & Moffat, K. (1996). *Science*, **274**, 1726–1729.
Teng, T.-Y. (1990). *J. Appl. Cryst.* **23**, 387–391.